

University of Texas Rio Grande Valley

ScholarWorks @ UTRGV

Biology Faculty Publications and Presentations

College of Sciences

1-2023

The photochemical evolution of polycyclic aromatic hydrocarbons and nontronite clay on early Earth and Mars

Nina Kopacz

Maria Angela Corazzi

Giovanni Poggiali

Ayla von Essen

Vincent Kofman

See next page for additional authors

Follow this and additional works at: https://scholarworks.utrgv.edu/bio_fac



Part of the [Biology Commons](#)

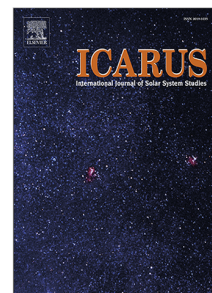
Authors

Nina Kopacz, Maria Angela Corazzi, Giovanni Poggiali, Ayla von Essen, Vincent Kofman, Teresa Fornaro, Hugo van Ingen, Eloi Camprubi, Helen E. King, John Brucato, and Inge Loes ten Kate

Journal Pre-proof

The photochemical evolution of polycyclic aromatic hydrocarbons and nontronite clay on early Earth and Mars

Nina Kopacz, Maria Angela Corazzi, Giovanni Poggiali, Ayla von Essen, Vincent Kofman, Teresa Fornaro, Hugo van Ingen, Eloi Camprubi, Helen E. King, John Brucato, Inge Loes ten Kate



PII: S0019-1035(23)00014-3
DOI: <https://doi.org/10.1016/j.icarus.2023.115437>
Reference: YICAR 115437

To appear in: *Icarus*

Received date: 15 October 2022
Revised date: 10 January 2023
Accepted date: 11 January 2023

Please cite this article as: N. Kopacz, M.A. Corazzi, G. Poggiali et al., The photochemical evolution of polycyclic aromatic hydrocarbons and nontronite clay on early Earth and Mars. *Icarus* (2023), doi: <https://doi.org/10.1016/j.icarus.2023.115437>.

This is a PDF file of an article that has undergone enhancements after acceptance, such as the addition of a cover page and metadata, and formatting for readability, but it is not yet the definitive version of record. This version will undergo additional copyediting, typesetting and review before it is published in its final form, but we are providing this version to give early visibility of the article. Please note that, during the production process, errors may be discovered which could affect the content, and all legal disclaimers that apply to the journal pertain.

© 2023 The Author(s). Published by Elsevier Inc. This is an open access article under the CC BY license (<http://creativecommons.org/licenses/by/4.0/>).

1 The photochemical evolution of polycyclic aromatic hydrocarbons 2 and nontronite clay on early Earth and Mars

3 Nina Kopacz^{a,*}, Maria Angela Corazzi^{b,c}, Giovanni Poggiali^{b,d}, Ayla von Essen^a,
4 Vincent Kofman^{e,f}, Teresa Fornaro^b, Hugo van Ingen^g, Eloi Camprubi^h, Helen E. King^a,
5 John Brucato^b and Inge Loes ten Kate^a

6 ^aDepartment of Earth Sciences, Utrecht University, Utrecht, the Netherlands

7 ^bINAF Astrophysical Observatory of Arcetri, Florence, Italy

8 ^cDepartment of Physics & Astronomy, University of Florence, Florence, Italy

9 ^dLESIA-Observatoire de Paris, Université PSL, CNRS, Sorbonne Université, Université de Paris, Meudon, France

10 ^eNASA Goddard Space Flight Center, Greenbelt, MD, USA

11 ^fAmerican University, Washington, DC, USA

12 ^gNMR Group, Bijvoet Centre for Biomolecular Research, Utrecht University, Utrecht, the Netherlands

13 ^hUniversity of Texas Rio Grande Valley, Edinburg, TX, USA

14 ARTICLE INFO

15 Keywords:

16 early Mars
17 polycyclic aromatic hydrocarbons
18 clays

19 ABSTRACT


The photochemical evolution of polycyclic aromatic hydrocarbons (PAHs), an abundant form of meteoritic organic carbon, is of great interest to early Earth and Mars origin-of-life studies and current organic molecule detection efforts on Mars. Fe-rich clay environments were abundant on early Earth and Mars, and may have played a role in prebiotic chemistry, catalyzing the breakdown of PAHs and freeing up carbon for subsequent chemical complexification. Current Mars is abundant in clay-rich environments, which are most promising for harboring organic molecules and have comprised the main studied features by the Curiosity rover in search of them. In this work we studied the photocatalytic effects of the Fe-rich clay nontronite on adsorbed PAHs. We tested the effect of ultraviolet radiation on pyrene, fluoranthene, perylene, triphenylene, and coronene adsorbed to nontronite using the spike technique, and *in situ* diffuse reflectance infrared Fourier transform (DRIFT) spectroscopy in a Mars simulation chamber. We studied the infrared vibrational PAH bands with first order reaction kinetics and observed an extensive decrease of bands of pyrene, fluoranthene, and perylene, accompanied by the formation of PAH cations, while triphenylene and coronene remained preserved. We further analyzed our irradiated samples with nuclear magnetic resonance (NMR). Our study showed certain PAHs to be degraded via the (photo)Fenton mechanism, even under a dry, hypoxic atmosphere. Using solar spectra representative of early Earth, early Mars, and current Mars surface illumination up to 400 nm, the processes occurring in our set up are indicative of the UV-induced photochemistry taking place in Fe-rich clay environments on early Earth and Mars.

20 1. Introduction

21 Polycyclic aromatic hydrocarbons (PAHs) represent 10-20% of cosmically available carbon (Tielens, 2013). PAHs
22 and PAH clusters are responsible for the 3-15 μm infrared emission bands, which have been observed in remarkably
23 similar quantities across the observable universe (Pendleton and Allamandola, 2002). Formed through combustion
24 processes in circumstellar regions, these compounds undergo gas phase processing in the interstellar medium when
25 subjected to ultraviolet (UV) and Lyman- α radiation and shock waves (Frenklach and Feigelson, 1989; Cherchneff
26 et al., 1992).

27 Once incorporated into ice and rock in small bodies like asteroids and comets, PAHs experience a wholly different
28 chemical evolution than in the gas phase. They can undergo hydrothermal alteration in the interiors of asteroids (Giese
29 et al., 2019) and radiative ice processing at the surfaces of comets (Kofman et al., 2018). PAHs eventually reach
30 planetary surfaces ferried by interplanetary dust particles (IDPs) and (micro)meteorites. Depending on their origin,

*Nina Kopacz

 k. a. kopacz@uu.nl (N. Kopacz)

ORCID(s):

The photochemical evolution of polycyclic aromatic hydrocarbons and nontronite clay on early Earth and Mars

49 the isotopic signatures of PAHs in meteorites may carry information on accretion processes and aqueous alteration
50 conditions (Lecasble et al., 2022).

51 The further photochemical evolution of PAHs delivered to a planetary surface environment by meteoritic sources is
52 of great interest to early Earth and Mars origin-of-life studies, as well as current organic molecule detection efforts on
53 Mars. Both early Earth and early Mars likely experienced high luminosity in the ultraviolet part of the solar spectrum,
54 the lack of ozone allowing the full range of UV between 200 and 400 nm to reach the surface (Cnossen et al., 2007;
55 Claire et al., 2012; Cockell, 2000). Currently the Martian atmosphere does little to attenuate the UV flux from 200-
56 400 nm, with an average mid-day flux at Gale Crater of 34.1 Wm^{-2} (Vicente-Retortillo et al., 2020; Razzell Hollis
57 et al., 2021).

58 Of prebiotic interest to both Earth and Mars are clay-rich environments, and the evolution of organic carbon
59 molecules within them. On Mars, clay environments are most promising for harboring organic molecules (Grotzinger
60 et al., 2014; Freissinet et al., 2015; Eigenbrode et al., 2018). Clay minerals on early Earth are posited to have played a
61 role in prebiotic molecular evolution (Cairns-Smith, 1966; Hartman, 1975). Bernal first speculated on the importance
62 of clays in this respect, because of their well-ordered arrangement, their large surface and interlayer adsorption capacity,
63 their shielding capacity against ultraviolet radiation, their ability to concentrate organic molecules, and their ability to
64 serve as polymerization templates (Bernal, 1949).

65 Abiogenesis-focused clay experiments have most often used montmorillonite, which has been shown to catalyze
66 a large variety of organic reactions involving small molecules and PAHs (Bujdak et al., 1994; Kumar et al., 2014;
67 Huang and Ferris, 2006; Juntunen et al., 2018), as well as serve in a protective capacity for small molecules in radiative
68 environments (Scappini et al., 2004). However, Fe-rich smectites, and in particular nontronite, are thought to have been
69 significantly more abundant on early Earth and Mars (Kloprogge and Hartman, 2022), and are indeed the dominant form
70 of smectite detected on Mars (Bibring et al., 2005; Murchie et al., 2009). Little research has investigated the catalytic
71 properties of these smectites, and it is unclear if the results obtained for montmorillonite can be directly translated to
72 nontronite and other Fe-rich smectites (Kloprogge and Hartman, 2022). Here we explore the photochemical evolution
73 of PAHs adsorbed to nontronite clay, and speculate on both of their roles in prebiotic carbon chemistry.

74 1.1. Delivery of PAHs to clay environments on early Earth

75 The annual flux of carbonaceous material (organic and inorganic) delivered by extraterrestrial sources to Earth is
76 currently 300 tonnes per year (Glavin et al., 2018) and could have been as high as 10 000 to 1 million tonnes per year in
77 the first 0.6 Ga of Earth's history (Whittet, 1997; Jenniskens et al., 2000). The significant volume of extraterrestrially
78 delivered organic matter begs the question of whether it was a source of molecules important for prebiotic chemistry.
79 Meteoritic organic matter is thought to be strongly associated with clay minerals in carbonaceous chondrites, wherein
80 complex chemical evolution may already take place (Pearson et al., 2002). Much of the literature has focused on small
81 molecules contained in meteorites, such as amino acids and nucleic acid bases, and their potential as a carbon source
82 for prebiotic chemistry on early Earth (e.g. Marty et al., 2013). However, 75% of extraterrestrial organic matter
83 in meteorites is in aromatic form (Sephton, 2002), and is more likely to survive the journey to a planetary surface,
84 during which much of the small molecules can be destroyed (Basiuk and Navarro-González, 1998; Basiuk et al., 1999).
85 PAHs could later be broken down into smaller, more biologically relevant and reactive molecules by photolysis and
86 photocatalysis in the ultraviolet radiation regime of early Earth (Ehrenfreund et al., 2006).

87 Though little is known about Earth's surface during the Hadean and early Archean, it is thought that the crust would
88 have consisted primarily of basalt and komatiite lavas containing peridotite-derived rocks high in Fe and Mg content
89 (O'Neil et al., 2008; Davies, 1992). The peridotite and komatiite rocks that made up the ocean floor and emerging
90 plateaus favored the formation of Fe-Mg clay minerals upon interaction with seawater and hydrothermal alteration.
91 The rocks would first react to trioctahedral phyllosilicates such as talc, kerolite, or stevensite-saponite, until increasing
92 weathering would cause these to destabilize and form dioctahedral Fe-rich clay minerals, with nontronite as the most
93 abundant species (Kloprogge and Hartman, 2022).

94 1.2. Delivery of PAHs to clay environments on Mars

95 The estimated current global carbon flux on Mars from cometary impacts is 13 tonnes per year within an order of
96 magnitude, and 50 tonnes per year from asteroids (Frantseva et al., 2018). The amount of organic material delivered
97 to the surface of Mars by IDPs and (micro)meteorites is estimated to be of the order of 1000 tonnes per year (Flynn,
98 1996; Flynn et al., 2004) and would have been higher in its early history.

The photochemical evolution of polycyclic aromatic hydrocarbons and nontronite clay on early Earth and Mars

99 On Mars, ancient sedimentary environments have been found with several tens of nanomoles of carbon compounds
100 (Grotzinger et al., 2014; Freissinet et al., 2015; Eigenbrode et al., 2018). Biological, geological, and meteoritic
101 sources are all possible for the refractory aromatic organic material from the Sheepbed lacustrine mudstones detected
102 by the Sample Analysis at Mars (SAM) instrument onboard the Curiosity rover (Eigenbrode et al., 2018). The
103 diverse molecular contributions in the SAM gas chromatography-mass spectrometry (GC-MS) data from Mojave
104 and Confidence Hills are consistent with the complex chemistry of meteoritic and geological organic matter and the
105 interactions that occur during pyrolysis of sediments (Moldoveanu, 2009). Coevolving volatiles analyzed above 500°C
106 in the Mojave and Confidence Hills analyses suggest the pyrolysis of geological refractory organic macromolecules
107 typically found in carbonaceous chondrites (Remusat et al., 2005; Okumura and Mimura, 2011).

108 The diversity of smectites on Mars includes nontronite, saponite, beidellite, and montmorillonite, with Fe/Mg-rich
109 clays dominating having formed by water-restricted alteration of the original basaltic and ultramafic rocks (Klopogge
110 and Hartman, 2022). Another theory suggests that primordial clays on Mars were formed when Mars' primary crust
111 reacted with a dense steam or supercritical atmosphere of water and carbon dioxide that was outgassed during magma
112 ocean cooling (Cannon et al., 2017). Such a mechanism would have formed a widespread coherent layer of clays on
113 the Martian surface during the pre-Noachian era.

114 The Martian rock record is abundant in preserved Noachian rocks. CheMin data from the Curiosity rover have
115 shown that ancient fluvio-lacustrine rocks in Gale crater contain up to 35 wt.% of clay minerals (Grotzinger et al.,
116 2014; Bristow et al., 2015). While the CheMin instrument has detected collapsed clays, i.e., with no interlayer water,
117 these clays were likely hydrated upon their formation on early Mars, before the changing environmental conditions
118 facilitated the desorption of structural water (Tu et al., 2021). The majority of clay minerals detected by orbital imaging
119 spectrometers are Fe/Mg smectites in 4 billion-year-old rocks (Bibring et al., 2005; Murchie et al., 2009). Nontronite
120 spectral signatures have been studied on the flanks of the central mount of Gale Crater (Poulet et al., 2014; Thomson
121 et al., 2011), and have comprised the main studied features by the Curiosity rover in its search for organic molecules.

122 1.3. The influence of clay environments on PAHs

123 The widespread abundance of nontronite on early Earth and Mars would have facilitated contact with PAHs after
124 their liberation from their meteoritic parent bodies. Nontronite has been shown to exhibit both photoprotective and
125 photocatalytic properties to adsorbed organic molecules in the presence of UV radiation, facilitating their preservation
126 or eventual removal (Fornaro et al., 2018b; Poch et al., 2015; dos Santos et al., 2016).

127 Fe-rich clays like nontronite exhibit catalytic properties: they are able to create electron-hole pairs where reaction
128 of the holes with adsorbed water molecules create OH radicals that can oxidize organic compounds, as first described
129 for heterogeneous catalysis on TiO₂ surfaces (Linsebigler et al., 1995; Fujishima et al., 2000). Electron-hole pairs can
130 also induce oxidation without creating free radicals by involving chemisorbed molecules that serve as electron hole
131 traps (Shkrob and Chemerisov, 2009; Shkrob et al., 2011a,b).

132 Photocatalysis has been shown to increase PAH degradation in aqueous environments under current terrestrial
133 conditions (Wen et al., 2002; Ohno et al., 2003; Dong et al., 2010a). Environmental pollution studies have highlighted
134 the photocatalytic effects of metal oxides and clays that facilitate the degradation of PAHs (Dong et al., 2010a,b).
135 However, PAHs bond to mineral grains via π -cloud interactions (Campisi et al., 2021, 2022). Experiencing only weak
136 bonds or long range interactions with their mineral substrates, the extent of photocatalytic effects on their degradation
137 in a dry, hypoxic environment without abundant (oxi)hydroxide radical production is questioned.

138 In this work we experimentally tested the effect of UV radiation on different PAHs adsorbed to nontronite clay
139 using the spike technique. Analyses were performed with *in situ* diffuse reflectance infrared Fourier transform (DRIFT)
140 spectroscopy and nuclear magnetic resonance (NMR).

141 2. Materials & Methods

142 We conducted our experiments at the INAF-Astrophysical Observatory of Arcetri, with an experimental setup in
143 which samples were irradiated for 6 hours under ambient temperature and a nitrogen atmosphere. DRIFT spectra were
144 recorded every hour, with more frequent measurements at the beginning of each experiment. The chemical evolution
145 of organic molecules was described with first-order reaction kinetics. We then extracted the organic fraction from the
146 samples and analyzed them with NMR at Utrecht University.

The photochemical evolution of polycyclic aromatic hydrocarbons and nontronite clay on early Earth and Mars

2.1. Sample preparation

The Fe-rich clay mineral used in our experiments was selected to be representative of both early Earth and Mars and because it exhibits known catalytic properties. Natural nontronite clay was purchased from the Clay Minerals Society's Source Clays Project, where it is designated NAU-2 and is described structurally as $M_{0.72}^{+}[\text{Si}_{7.55}\text{Al}_{0.45}][\text{Fe}_{3.83}\text{Mg}_{0.05}]\text{O}_{20}(\text{OH})_4$ (Keeling et al., 2000). Prior to the experiments the nontronite sample needed to be crushed to obtain a grain size of $\sim 2 \mu\text{m}$. Since manual grinding of a clay may introduce torque, preferentially straining the mineral grains in the sample, reducing tensile strength and ultimately introducing structural changes, the nontronite was ground using a Herzog HP-MA automatic pulverizing mill equipped with a tungsten-carbide vessel. This mill allows the total pressing force to be program-controlled, and ensures that no particular sheer direction is imposed on the clay lattice (Herzog, 2022).

The indigenous organics present in the clay could be removed with organic solvent washing cycles. However, this could also remove the interlayer water. Though on current Mars the clays detected are collapsed, the clays on early Earth and Mars would have likely had water in their interlayer spaces. As we don't have insight into the potential alteration of the nontronite structure due to known clay organic removal techniques (Fornaro et al., 2020) and the readmittance of water with our ensuing spike technique, we chose to use the clay in its natural state. Other studies have also chosen not to remove the indigenous organics from nontronite (dos Santos et al., 2016). We opted instead to track the chemical evolution of these organics throughout the experiment.

The PAHs used for the experiments were pyrene, perylene, fluoranthene, triphenylene, and coronene, which have all been found in meteorites (Sephton, 2002). They were purchased from Sigma Aldrich and had a purity of 98%. We adsorbed pyrene, fluoranthene, and triphenylene individually to the nontronite powder via the incipient wetness impregnation technique (Fornaro et al., 2018a), in which a molecule in solution is added to the mineral sample until it becomes a thick slurry. The volume of the solution is thus equal to the mineral porous volume. To this end we dissolved pyrene, fluoranthene, and triphenylene in toluene, which does not alter the clay mineral structure unlike other solvents such as methanol. The molecules in solution were deposited on nontronite samples to achieve a 1:100 molecule to mineral mass ratio. This ratio produced adequate infrared spectra while allowing the PAH to dry in a way that appeared evenly and thinly spread across the mineral surfaces, instead of forming large crystals as was the case when deposited in larger amounts. The samples were left to dry overnight at room temperature in a chemical hood before being measured with DRIFT spectroscopy.

Perylene and coronene do not dissolve readily in toluene, and thus they cannot be deposited via the incipient wetness technique. Instead we mechanically ground each PAH individually with the mineral powder, with the assumption that the work introduced by grinding resulted in physisorption of the two species. To obtain adequate infrared spectra (with the same intensity of organic peaks as in the samples treated with the incipient wetness technique), the molecule to mineral ratio needed to be 1:10. It should be noted that for the nontronite samples, the mechanical grinding may introduce structural changes to the mineral. However, this is not apparent in the IR data, and no clear trends between the preparation methods were found in further analyses, thus the nontronite is assumed to be identical in all samples.

For pure PAH irradiation experiments, triphenylene, perylene and coronene were introduced into the experimental apparatus directly from the bottle without any further grinding. Pyrene and fluoranthene had a larger crystal size so were first ground and then introduced into the setup. An overview of the PAHs and the experiments performed with each can be seen in Table 1.

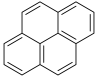
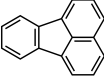
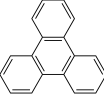
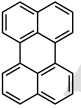

2.2. Experimental setup

The experimental setup at INAF-Astrophysical Observatory of Arcetri allows for the *in situ* monitoring of infrared spectra of samples subjected to UV irradiation. The apparatus consists of a Bruker *Vertex 70v* FTIR double pendulum spectrometer with a Harrick *Praying MantisTM* Diffuse Reflection Accessory for DRIFT measurements (Figure 1). The spectrometer is interfaced with a Newport Oriel 300 W Xenon arc discharge lamp with a spectral range of 200-930 nm, which is considered a good analog source for the UV that would have reached the surface of early Earth and Mars. The total UV flux of the lamp in the spectral range of 200-400 nm is 1.94×10^{16} photons s^{-1} , as measured by a single monochromator Spectro 320 scanning spectrometer (Instrument System) (Fornaro et al., 2018a). We work in this spectral range because here the molecular absorption is higher. The radiation is focused by an optical fiber from the lamp to the spectrometer with a spot size of $800 \mu\text{m}$ onto one of two sample holders: one holder designated 'large' with radius 0.5 cm, and the other holder designated 'small' with a radius of 0.15 cm. For a spectral range of 200-400 nm, this gives a UV flux of 141 Wm^{-2} for the large sample holder and 1570 Wm^{-2} for the small sample holder, as compared to the average mid-day flux at Gale Crater on Mars of 34.1 Wm^{-2} , calculated using the COMIMART radiative transfer

The photochemical evolution of polycyclic aromatic hydrocarbons and nontronite clay on early Earth and Mars

Table 1

Overview of experiments performed. Samples were irradiated under a 300 W Xe arc lamp in a chamber at ambient temperature under a nitrogen atmosphere.

PAH	pyrene	fluoranthene	triphenylene	perylene	coronene
formula	$C_{16}H_{10}$	$C_{16}H_{10}$	$C_{18}H_{12}$	$C_{20}H_{12}$	$C_{24}H_{12}$
					
nontronite sample preparation	incipient wetness impregnation	inc. wetness impregnation	inc. wetness impregnation	manual grinding	manual grinding
irradiation pure	6 h at 1570 Wm^{-2} (200-400 nm)				
irr. on nontronite	6 h at 141 Wm^{-2} (200-400 nm)				
analyses	FTIR, NMR	FTIR, NMR	FTIR, NMR	FTIR	FTIR

199 model with data from the UV sensor on the Rover Environmental Monitoring Station (REMS) on board the Curiosity
200 rover (Vicente-Retortillo et al., 2015; Razzell Hollis et al., 2021).

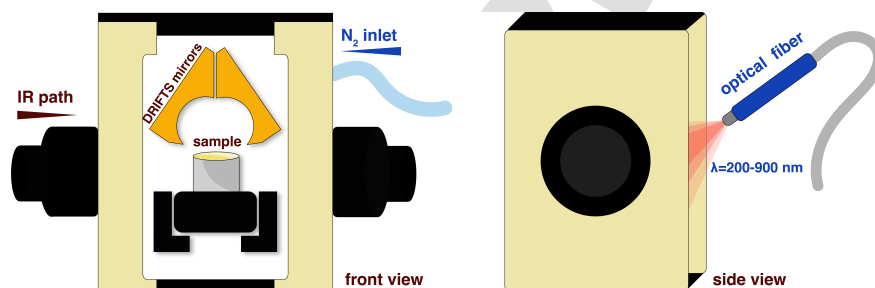


Figure 1: Schematic of the experimental setup at INAF-Astrophysical Observatory of Arcetri. The apparatus allows for the *in situ* monitoring of infrared spectra of samples subjected to UV irradiation.

201 With this apparatus the modification of the infrared spectrum of a sample due to UV irradiation can be monitored
202 at regular time intervals *in situ* without moving the sample itself. The reference spectrum for each PAH, recorded prior
203 to the experiment, can be seen in Figure S1 in Appendix A. DRIFT spectroscopy measurements were taken in steps of
204 increasing seconds for the first five minutes of irradiation, in steps of increasing minutes for the first hour, and every
205 hour for six hours. The evolution of the PAH molecules could thus be seen in real time, with photochemical degradation
206 manifesting itself as the decrease in peak sizes or the formation of new peaks, indicating bond breakage or new species
207 formation, respectively.

208 2.3. FTIR Analysis

209 PAH infrared spectra contain a cacophony of absorption peaks due to the many vibrational modes: ring deformation,
210 C-H out-of-plane (oop) bend, C-H in-plane (ip) bend, C-C stretch, C=C stretch, and C-H stretch. In this work the
211 individual peaks were grouped in these categories for analysis, and the C-H in-plane bend and C-C stretch were
212 grouped together since many of the bands overlap. Peak assignments were taken from reference spectra from the
213 Spectral Database of Organic Compounds (SDBS) (SDBS, 2022) and the NASA Ames PAH IR Spectroscopic Database
214 (Boersma et al., 2014; Bauschlicher et al., 2018; Mattioda et al., 2020a). The peak assignments can be seen in Table
215 S1 in Appendix A.

The photochemical evolution of polycyclic aromatic hydrocarbons and nontronite clay on early Earth and Mars

216 The area of each peak can be seen as proportional to the amount of molecules with that vibrational mode. The peak
 217 areas were plotted against time, and the destruction or formation rates, the half-lives, and cross sections were calculated
 218 following first order kinetics relations (Cottin et al., 2003; ten Kate et al., 2005). First order kinetics assume a one-to-
 219 one interaction between one UV photon and one broken linkage in a molecule. Not all of the peaks investigated were
 220 possible to fit with one exponential function, indicating it might take more than one photon to break the corresponding
 221 bond, or multiple pathways take place. Multiphoton processes in which a PAH absorbs a second photon before it has
 222 radiated the energy of the first photon away have a low probability but can be important as well (Tielens, 2008). Such
 223 processes were not taken into account in this analysis.

The destruction rate β is calculated fitting the following first order rate equation,

$$\frac{A(t)}{A_0} = Be^{-\beta t} + C \quad (1)$$

224 where A_0 is the area of the peak at time $t = 0$, β is the degradation rate of the peak, B is a coefficient describing
 225 the fraction of the sample which has interacted with the radiation, and C is a coefficient describing the fraction of
 226 the sample which has not interacted with the radiation. The radiation only penetrates a few microns into the sample,
 227 whereas the IR laser penetrates much further into the sample. $B + C$ should thus equal 1.

The equation for the destruction half-life $t_{d1/2}$, or the time it takes for half of the material to be destroyed, is

$$t_{d1/2} = \frac{\ln(2)}{\beta} \quad (2)$$

228 where β is the degradation rate.

The cross section describes the probability of interaction between the molecule and the UV radiation. Thus the
 higher the cross section, the higher the chance that there will be an interaction. The destruction cross section is defined
 as

$$\sigma_d = \frac{\beta}{\Phi} \quad (3)$$

229 where β is the degradation rate and Φ is the flux of the lamp over a specified wavelength range.

Similarly, the formation rate of new species is calculated by fitting the following first order rate equation,

$$\frac{A(t)}{A_{max}} = 1 - e^{-\alpha t} \quad (4)$$

230 where A_{max} is the maximum peak area and α is the formation rate of the peak.

231 Having obtained the formation rate, we can calculate the formation half-life $t_{f1/2}$, or the time it takes for half of
 232 the reaction products to form, with $t_{f1/2} = \frac{\ln(2)}{\alpha}$. The formation cross-section is then $\sigma_f = \frac{\alpha}{\Phi}$.

233 2.4. NMR Analysis

234 After irradiation we recovered the samples from the setup and stored them in Eppendorf tubes for further proton
 235 NMR analysis. This was a qualitative analysis in order to see whether the irradiated samples contained any reaction
 236 products, and whether the characteristic PAH peaks showed significant changes.

237 We extracted the organic fraction from the nontronite samples by incubating the samples in a bath at 60°C in a
 238 3:1 solution of HPLC-grade methanol and chloroform. The samples were then centrifuged at 1500 rpm for 8 min. The
 239 supernatant was removed and passed through a syringe filter to eliminate any residual mineral, and subsequently dried
 240 under nitrogen overpressure.

241 PAH standards, pure PAH samples, and extracted samples were suspended in fully deuterated chloroform and
 242 analyzed using a 600 Bruker NMR. Deuterated chloroform was used as only non-polar breakdown products were
 243 expected from the irradiation of PAHs in a dry, hypoxic environment, where there is little water and oxygen to generate
 244 polar compounds. Standard ^1H 1D spectra were acquired using the zg pulse sequence, using 2.7 s acquisition time, 4
 245 sec recycle delay and 256 scans (total measurement time 30 min per 1D). Spectra were processed using exponential
 246 line broadening of 0.3 Hz before Fourier transform using Bruker Topspin and plotted in MeRestNova for the paper
 247 figures. We performed this analysis only on pyrene, fluoranthene, and triphenylene, as perylene and coronene were not

The photochemical evolution of polycyclic aromatic hydrocarbons and nontronite clay on early Earth and Mars

Table 2

Nontronite infrared bands and assignments, taken from Madejová (2003) and Frost et al. (2002).

peak	band (cm ⁻¹)	vibrational mode
1	475	Si-O-Si bend
2	677	Fe-O oop bend
3	1200	Si-O stretch
4	1630	O-H bend
5	3580	O-H stretch

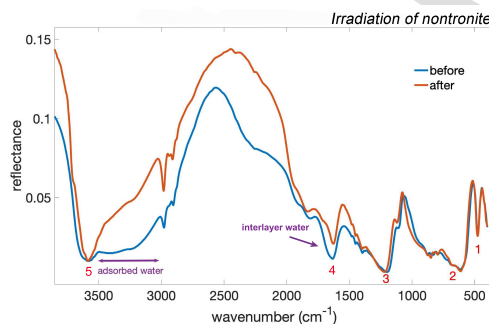


Figure 2
DRIFT spectrum of nontronite before and after irradiation. Numbered peaks correspond to vibrational modes in Table 2.

248 sufficiently soluble in chloroform. The NMR spectra of PAHs irradiated on nontronite were compared to the PAHs
249 irradiated pure, the PAH standards, and the experimental blanks, which consisted of the extraction solvent that had
250 been passed through a syringe filter, then dried and resuspended in deuterated chloroform.

251 3. Results

252 3.1. Irradiation of nontronite

253 The infrared spectrum of pure nontronite exhibited some changes after 6 h of irradiation. The Si-O-Si, Fe-O, and
254 Si-O infrared bands (listed in Table 2 and denoted by red numbers in Figure 2), did not show significant changes. The
255 O-H stretching band at 3580 cm⁻¹ did narrow after irradiation as a consequence of desorption of water physisorbed
256 on the clay, which is responsible for the broader band observed pre-irradiation in the same region and indicated by the
257 purple line in Figure 2. The band at 1630 cm⁻¹ is attributed to the O-H bending of water in the nontronite interlayer
258 space (Frost et al., 2002). We observe the decrease and shift of this band as some of the interlayer water is desorbed
259 through irradiation. The bands at ~2900 cm⁻¹ indicate C-H stretching in minor organic contaminants in the clay. These
260 were not removed from the clay prior to the experiment in order to avoid possible alterations of the clay structure that
261 might be caused by treatments usually employed to remove organics. The C-H stretching bands became more prominent
262 post-irradiation as the absorbance of water decreased, revealing the bands of the nontronite spectrum.

263 3.2. Irradiation of PAHs

264 We monitored the irradiation of PAHs *in situ* with DRIFT spectroscopy, with measurements taken in steps of
265 increasing seconds for the first five minutes of irradiation, in steps of increasing minutes for the first hour, and every
266 hour for six hours. All PAHs were irradiated pure and adsorbed to nontronite (Table 1).

267 Figure 3 shows the FTIR spectrum of fluoranthene adsorbed to nontronite before irradiation (in blue) and after
268 6 h of irradiation (in orange), where all of its characteristic peaks have decreased or disappeared entirely, revealing
269 the underlying spectrum of nontronite. The nontronite band at 3580 cm⁻¹ (O-H stretch, marked with a dotted circle
270 in Figure 3), which was obscured by the more prominent fluoranthene spectrum prior to irradiation, is visible post-
271 irradiation. We modeled the decay of peaks with Equations 1-4. The decay parameters of fluoranthene bands are listed
272 in Table 3. The C-H in-plane bend and C-C stretch were grouped in one category, since many of the bands overlap. The
273 parameters for the different bands are in a similar range and were averaged to give parameters for the total molecule.

274 We observed the degradation of perylene when adsorbed to nontronite and exposed to UV for 6 h (Figure 4a), as
275 well as the growth of some peaks (Figure 4b). The perylene bands that decreased did so at similar rates, though many
276 of the perylene bands could not be modeled with Equations 1-4 (Table S1, Figure S6 in Appendix A), and were thus not
277 included in the analysis. The formation of two bands in the C=C range is pointed out with red arrows in Figure 4a, and
278 manifests as the growth and rightward shift of bands at 1543 cm⁻¹ and 1346 cm⁻¹ (Figure 4b). The formation kinetics
279 of new bands is shown in Figure 4c, and is consistent with the formation of perylene cations (Szczepanski et al., 1993).
280 However, there should also be a rightward shift and growth of the peak at 1334 cm⁻¹ to 1318 cm⁻¹, which we do not
281 observe. This could be due to the stifling of certain vibrations because of mineral matrix or PAH crystal effects, which

The photochemical evolution of polycyclic aromatic hydrocarbons and nontronite clay on early Earth and Mars

Table 3

Degradation kinetics of UV-irradiated fluoranthene ($C_{16}H_{10}$) adsorbed to nontronite. Parameters were calculated with Equations 1-4.

mode	$t_{d1/2}$ (min)	σ_d ($\times E^{-19} cm^2$)
ring deformation	83 ± 21	3 ± 1
C-H oop bend	69 ± 32	10 ± 4
C-H ip bend/ C-C stretch	62 ± 13	5 ± 1
C=C stretch	74 ± 17	4 ± 1
total molecule	72 ± 20	6 ± 2

oop: out-of-plane, ip: in-plane

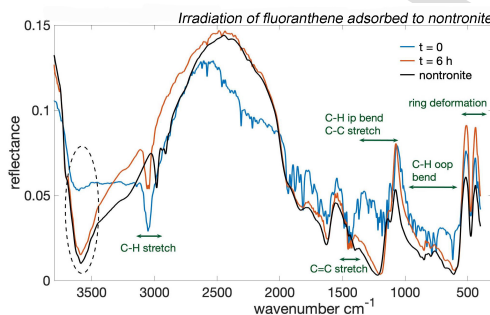


Figure 3

FTIR reflectance spectrum of fluoranthene adsorbed to nontronite before (blue) and after (orange) irradiation, and nontronite post-irradiation (black). The dotted circle marks the OH-stretch of nontronite at 3580 cm^{-1} .

do not allow the PAHs to vibrate freely as they would in the gas phase. This could also explain the differences in the intensities of the 1543 cm^{-1} and 1346 cm^{-1} bands between our experiments and those reported in the literature for gas phase or matrix-isolated species. In addition, the area around 1318 cm^{-1} is very crowded with intense underlying nontronite bands. This could obscure detection of the 1318 cm^{-1} , if it is present.

The formation of PAH ion peaks generally show an initial growth before plateauing off or slightly decreasing due to photobleaching of the ions (Mattiola et al., 2020a; Hudgins and Allamandola, 1997; Hudgins and Sandford, 1998), as seen in our results in Figure 4c. Photoproducts, on the other hand, would increase linearly with time (Mattiola et al., 2020a), and any PAH hydrogenation would be associated with the growth of C-H stretching bands in the $2800\text{--}3000\text{ cm}^{-1}$ region (Cruz-Diaz et al., 2020), which we do not observe as the perylene C-H band in that region is degraded (Table 5). However, the growth of the 1543 cm^{-1} and 1346 cm^{-1} bands could alternatively be indicative of C-H bending bands (Mattiola et al., 2020b), suggesting the hydrogenation of the perylene molecules. Whether we are observing the formation of perylene cations or rather the hydrogenation of perylene molecules could be hinted at by which of the two are more stable on the nontronite surface. Previous work has shown that PAH radical cations can persist on irradiated clay surfaces for several hours in an oxidic environment, before they are further broken down by reactive oxygen species (Jia et al., 2019). As the atmosphere in our experiments is largely anoxic, we could expect both perylene cations and hydrogenated perylene to remain stable for the length of the experiment.

When pure PAHs were irradiated, only the spectrum of triphenylene exhibited changes (Figure 5a), while no changes were observed in the spectra of pyrene, perylene, fluoranthene, and coronene (Figure S2 in Appendix A). While pure triphenylene manifested peak degradation during irradiation, triphenylene on nontronite exhibited peak growth (Figure 5b) at similar rates for all peaks. This indicates preservation of the molecule: the slight growth of peaks at the beginning of the experiment is probably due to the rearranging of the PAH molecules in the sample due to minimal heating effects. The peak degradation and growth kinetics of triphenylene are compared in Table 4.

The reaction kinetics of all PAHs adsorbed to nontronite are listed in Table 5. Pyrene, fluoranthene, and perylene were degraded in the presence of UV and nontronite, with at least half of the PAHs removed after 6 h of irradiation. Triphenylene and coronene exhibited peak growth in the presence of UV and nontronite, indicating the retention of the PAHs in the samples during 6 h of irradiation. Again, the growth of the IR bands is rather due to the rearranging of the PAH molecules in the sample at the start of the experiment rather than the formation of new products, as there are no new peaks forming. Desorption of PAH molecules by the UV lamp or the IR beam was discounted, based on temperature measurements of the sample area and previous work in the setup, which has not encountered issues with such effects (Potenti et al., 2018; Poggiali et al., 2020; Fornaro et al., 2018a). The spectra pre- and post-irradiation of all UV-irradiated PAHs adsorbed to nontronite are shown in Figure S3 and their reaction kinetics in Figures S4-S6 in Appendix A.

The clay-related organic contaminants at $\sim 3000\text{ cm}^{-1}$ (Figure 2), which were not removed from the clay, were also subject to the irradiation experiments. The degradation of the band at $\sim 3000\text{ cm}^{-1}$ belonging to the contaminants may contribute slightly to the parameters calculated for the C-H stretch of perylene, triphenylene, and coronene. However,

The photochemical evolution of polycyclic aromatic hydrocarbons and nontronite clay on early Earth and Mars

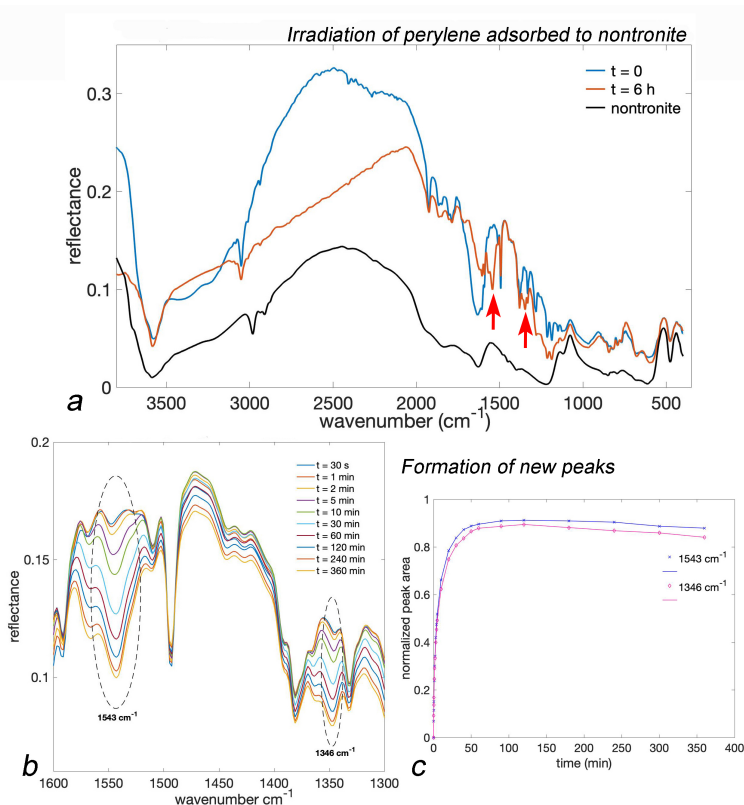


Figure 4: FTIR spectra of perylene adsorbed to nontronite before and after irradiation, compared to the spectrum of nontronite post-irradiation (a), (b) formation of new peaks during irradiation of perylene (indicated by red arrows in (a)), (c) reaction kinetics of new peaks shown in (b).

317 the overall behavior of the bands is reflecting changes in the PAH molecules, given that their kinetics are in line with
 318 the kinetics of the other bands (Table 5). For pyrene and fluoranthene the kinetics of the band at ~ 3000 cm⁻¹ were
 319 discounted, as they exhibited behavior much different to that of the other bands. This may indicate that the behavior of
 320 that band was dominated by the eventual degradation of the organic clay-related contaminants.

3.3. Extractions of PAHs post-irradiation

322 Pyrene, fluoranthene, and triphenylene samples recovered from the irradiation experiments were further analyzed
 323 with NMR (Figure 6). The NMR spectra of PAHs irradiated on nontronite were compared to the PAHs irradiated pure,
 324 the PAH standards, and the experimental blanks. Note that the NMR studies are purely qualitative.

325 The spectra of pure, irradiated, and clay-irradiated PAHs were superimposed (Figures 6a, c, e) and scaled to match
 326 the intensities of the characteristic PAH aromatic peaks. This allowed us to detect changes in relative peak intensities
 327 indicating degradation. In the pyrene and fluoranthene clay-irradiated samples (Figure 6a, c), the characteristic PAH
 328 peaks decreased strongly in intensity relative to the small aromatic peaks in the region, indicating the degradation
 329 of the PAHs. These smaller signals surrounding the PAH peaks are likely from aromatic impurities as they are also
 330 present in the pure PAH samples but at much lower intensity to the pure PAH signals. Based on the change in relative
 331 intensity, about 30% of pyrene and 40% of fluoranthene were degraded.

332 Further analysis of the spectra showed that a new shoulder formed on the clay-irradiated pyrene peak at 8.18 ppm,
 333 indicating the presence of a possible partly degraded PAH intermediate (pointed out with a black arrow in Figure 6a).
 334 A few more new peaks appeared in the clay-irradiated samples at ~ 3.5 ppm (the range of alcohols) in the pyrene and

The photochemical evolution of polycyclic aromatic hydrocarbons and nontronite clay on early Earth and Mars

Table 4

Reaction kinetics of UV-irradiated triphenylene pure and adsorbed to nontronite. Parameters were calculated with Equations 1-4.

triphenylene	pure		on nontronite	
mode	$t_{d1/2}$ (min)	$\sigma_d \times E^{-19}(\text{cm}^2)$	$t_{f1/2}$ (min)	$\sigma_f \times E^{-19}(\text{cm}^2)$
ring deformation	200±120	0.15±0.08	13±4	22±9
C-H oop bend	230±130	0.14±0.06	17±7	17±8
C-H ip bend/C-C stretch	97±37	0.28±0.09	8±2	62±32
C=C stretch	110±33	0.34±0.01	7±3	40±20
C-H stretch	94±29	0.3±0.1	10±4	29±14
total molecule	150±69	0.23±0.09	11±4	34±17
flux (Wm^{-2})	1570		141	

oop: out-of-plane, *ip*: in-plane, $t_{d1/2}$: destruction half-life, σ_d : destruction cross section, $t_{f1/2}$: formation half-life, σ_f : formation cross section

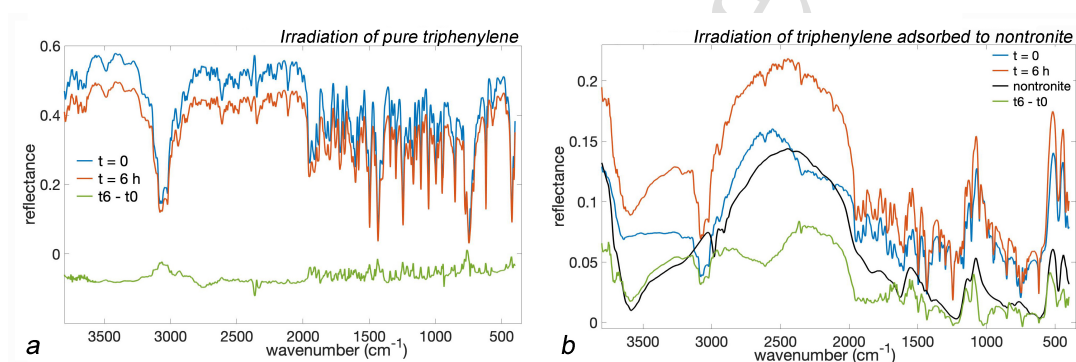


Figure 5

FTIR spectra of triphenylene ($\text{C}_{18}\text{H}_{12}$) irradiated pure (a) and adsorbed to nontronite (b). The nontronite spectrum post-irradiation is shown in black, and the difference spectra of triphenylene (spectrum at $t=0$ subtracted from spectrum at $t=6$) are shown in green.

335 triphenylene samples (indicated by black arrows in Figures 6b, f). Fluoranthene already has this shift in its standard
 336 spectra, and a shift here could also be attributed to indigenous organics within the clay structure. The other new signals
 337 in the clay-irradiated samples are accounted for by the experimental blanks.

338 4. Discussion

339 4.1. Effect of UV on nontronite

Fe-rich clays like nontronite can exhibit catalytic properties in the presence of UV radiation: they can create electron-hole pairs that can react either with adsorbed water molecules creating hydroxyl radicals, or with chemisorbed molecules that serve as electron hole traps (Linsebigler et al., 1995; Fujishima et al., 2000; Shkrob et al., 2011a,b). The presence of water physisorbed on the clay and the structural water of the clay could result in the production of OH radicals that may facilitate the Fenton mechanism (Fenton, 1894). The Fenton reaction results in the oxidation of Fe^{2+} to Fe^{3+} ,



The photochemical evolution of polycyclic aromatic hydrocarbons and nontronite clay on early Earth and Mars

Table 5

Reaction kinetics of UV-irradiated PAHs adsorbed to nontronite. Parameters were calculated with Equations 1-4. The destruction half-life ($t_{d1/2}$), destruction cross section (σ_d), formation half-life ($t_{f1/2}$) and formation cross section (σ_f) are given for each vibrational mode for the corresponding PAH, and averaged for the total molecule. The C-H in-plane bend and C-C stretch are grouped in one category, since many of the bands overlap.

	PAH	pyrene	fluoranthene	perylene	PAH	triphenylene	coronene
mode	degradation	C ₁₆ H ₁₀	C ₁₆ H ₁₀	C ₂₀ H ₁₂	retention	C ₁₈ H ₁₂	C ₂₄ H ₁₂
ring	$t_{d1/2}$ (min)	220±65	83±21	n/a	$t_{f1/2}$ (min)	13±4	4±3
deformation	$\sigma_d \times E^{-19}(\text{cm}^2)$	1.4±0.7	3±1	n/a	$\sigma_f \times E^{-19}(\text{cm}^2)$	22±9	81±87
C-H	$t_{d1/2}$ (min)	80±9	69±31	77±33	$t_{f1/2}$ (min)	17±7	n/a
oop bend	$\sigma_d \times E^{-19}(\text{cm}^2)$	3.8±0.8	10±4	4±2	$\sigma_f \times E^{-19}(\text{cm}^2)$	17±8	n/a
C-H ip bend	$t_{d1/2}$ (min)	180±42	62±13	49±10	$t_{f1/2}$ (min)	8±2	n/a
C-C stretch	$\sigma_d \times E^{-19}(\text{cm}^2)$	1.6±0.5	5±1	6±2	$\sigma_f \times E^{-19}(\text{cm}^2)$	62±32	n/a
C=C	$t_{d1/2}$ (min)	210±55	74±17	n/a	$t_{f1/2}$ (min)	7±3	2.5±0.6
stretch	$\sigma_d \times E^{-19}(\text{cm}^2)$	1.4±0.5	4±1	n/a	$\sigma_f \times E^{-19}(\text{cm}^2)$	40±20	120±43
C-H	$t_{d1/2}$ (min)	n/a	n/a	40±10	$t_{f1/2}$ (min)	10±4	7±3
stretch	$\sigma_d \times E^{-19}(\text{cm}^2)$	n/a	n/a	7±2	$\sigma_f \times E^{-19}(\text{cm}^2)$	29±14	39±22
total molecule	$t_{d1/2}$ (min)	170±43	72±20	55±17	$t_{f1/2}$ (min)	11±4	4±2
	$\sigma_d \times E^{-19}(\text{cm}^2)$	2.0±0.6	6±2	6±2	$\sigma_f \times E^{-19}(\text{cm}^2)$	34±17	79±51

oop: out-of-plane, ip: in-plane

$t_{d1/2}$: destruction half-life, σ_d : destruction cross section

$t_{f1/2}$: formation half-life, σ_f : formation cross section

The photo-Fenton reaction is enhanced by UV light at wavelengths <350 nm, producing additional OH radicals, and leading to Fe³⁺ reduction (Ruppert et al., 1993),



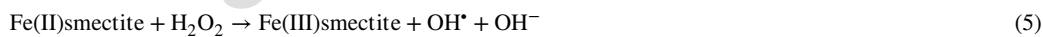
and regeneration of the catalyst,



In our experiments, Reactions 2 and 3 described above can generate Fe²⁺ and OH, producing H₂O₂, and facilitating the Fenton mechanism leading to the reduction of the clay,



The clay may be subject to subsequent reoxidation by H₂O₂ Jia et al. (2012); Yap et al. (2011),



The photochemical evolution of polycyclic aromatic hydrocarbons and nontronite clay on early Earth and Mars

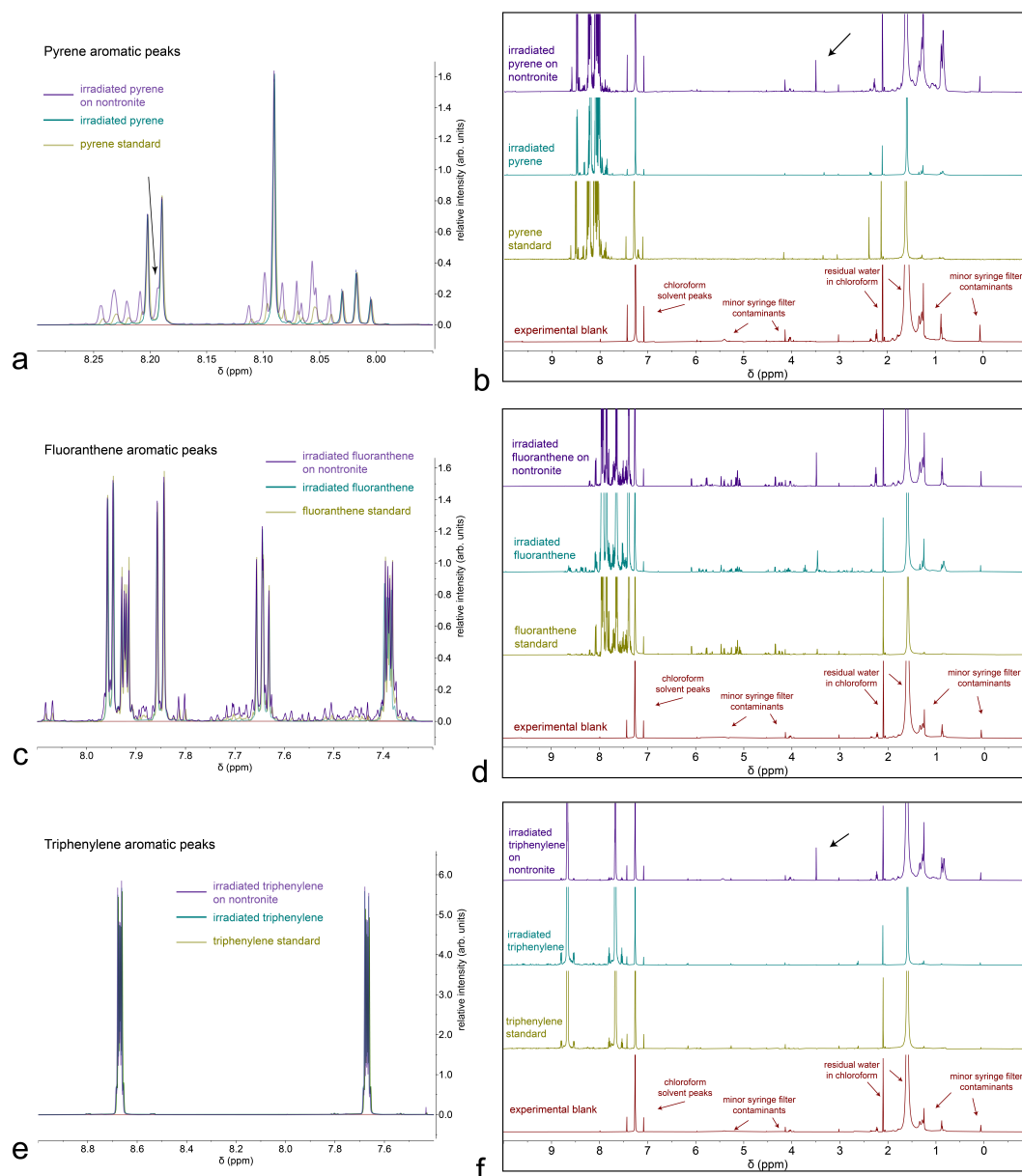


Figure 6: NMR data of irradiated samples. Pure PAHs and PAHs extracted from clay samples are compared to PAH standards and experimental blanks. (a-b) spectra of pyrene, (c-d) spectra of fluoranthene, (e-f) spectra of triphenylene. The data are normalized to the intensity of the PAH peaks. New peaks or shoulders are marked with black arrows. The superimposed spectra were scaled to match the intensities of the characteristic PAH aromatic peaks, revealing potential changes in relative peak intensities.

The photochemical evolution of polycyclic aromatic hydrocarbons and nontronite clay on early Earth and Mars or in the presence of oxygen,



340 forming superoxide radicals (Sýkora, 1997).

341 The OH radicals and H₂O₂ can further catalyze the photo-Fenton reaction and can oxidize PAHs adsorbed to the
342 mineral surface. The hypoxic experimental conditions in our experiments likely inhibit Reaction 6, in part stifling
343 subsequent oxidation of reduced nontronite. Nonetheless, the Fenton mechanism can proceed following the ionization
344 of surface and interlayer water molecules and OH groups by UV radiation. This is supported by the decrease in the O-H
345 bending and stretching bands in the nontronite IR spectrum post irradiation (Figure 2). The removal of interlayer water
346 from the clay is indicative of the processes occurring on Mars, where the CheMin instrument has detected collapsed
347 clays, i.e., with no interlayer water (Tu et al., 2021). The interlayer water was likely removed from these clays over
348 time, facilitated by the changing environmental conditions, particularly the increasingly harsh radiative environment.

349 The catalytic activity of nontronite is excellent over a wide pH range, with nontronite remaining both chemically
350 and mechanically stable, with no measurable Fe leaching, damage to the structure, or noticeable loss of activity (Liu
351 et al., 2014). Reduction in nontronite occurs to the greatest extent in the octahedral sheet iron and oxidation in the
352 tetrahedral sheet iron (Geatches et al., 2012). Reduction of octahedral iron causes a change in specific surface area
353 of the smectite sheets, (Lear and Stucki, 1989) which can reduce the interlayer spacing and trap interlayer cations,
354 ultimately changing the reactivity of the clay.

355 Fe²⁺ and Fe³⁺ act as photocatalysts via the Fenton mechanism at low pHs (≤ 4) (Fenton, 1894). Nontronite has
356 the potential to have high surface acidity, due to exchangeable cations in its interlayer space (Laszlo, 1987). This will
357 be more important in a dry environment, with no water molecules to react with to reduce the acidity. Carbocations
358 formed here can further react with interlayer water to produce alcohols and ethers (Theng, 2018; Adams et al., 1979;
359 Nagendrappa et al., 2002). This may explain the appearance of additional peaks at ~ 3.5 ppm in our NMR spectra of
360 the organic extractions of clay-irradiated samples (Figure 6).

361 Conversely, Fe-rich minerals can be strong absorbers of UV light, which can provide protection against radiation
362 damage (Pierson et al., 1993; Gauger et al., 2015). Nontronite has been shown to exhibit a photoprotective effect
363 on adsorbed amino acids when irradiated with UV under current Martian surface conditions (Poch et al., 2015; dos
364 Santos et al., 2016). These results suggest that photoprotection by nontronite is not only due to mechanical shielding
365 (elevated because of the clay's high surface area and small pore sizes) (dos Santos et al., 2016), but also caused by
366 stabilizing interactions between the molecules and the mineral surface, which allow absorbed energy to dissipate and
367 photodissociated molecules to recombine (Poch et al., 2015).

368 Nontronite's high surface area also creates more sites for PAH adsorption to the clay and potential for PAHs to
369 experience the catalytic effects of Fe in the clay. Thus nontronite can exhibit both photoprotective and photocatalytic
370 effects, with the dominant effect seeming to vary per PAH, as described in the next section.

371 4.2. Effect of UV on PAHs

The adsorption of PAHs to Fe-rich clay minerals is likely accompanied by the formation of "cation- π " interactions at the active sites, inducing electron transfer from PAHs to surface cations (Jia et al., 2018). This would result in oxidation of the PAH,



372 and further oxidation of the PAH by radicals and H₂O₂ produced in Reactions 3-6.

373 In previous work, the photodegradation of pyrene in solid state on various Fe oxide surfaces had a half-life of 3
374 to 4 hours depending on the Fe oxide, calculated by extracting and measuring pyrene concentration over irradiation
375 time (Wang et al., 2009). Pyrene was identified as an intermediary reaction product by gas chromatography-mass
376 spectrometry (GC-MS). Similarly, the photodegradation of pyrene on TiO₂ and soil surfaces was studied, and all loss
377 of pyrene was attributed to ionization by the Fenton mechanism (Zhang et al., 2008, 2010).

378 The photodegradation of phenanthrene under visible light (380-780 nm) was found to follow a pseudo-first-
379 order kinetic model when adsorbed to smectite saturated with Fe³⁺ cations, with 100% loss after 6 h of irradiation
380 (Jia et al., 2012). They attributed the degradation to the photo-Fenton effect, wherein hydroxyl radicals and singlet

The photochemical evolution of polycyclic aromatic hydrocarbons and nontronite clay on early Earth and Mars

381 oxygen preferentially attack phenanthrene at positions 9 and 10, eventually leading to the production of 9,10-
382 Phenanthrenequinone, phthalate, diisobutyl phthalate and various alkanes, such as esters, alkanic acids, alkanols,
383 alkanes, and dioxanes.

384 Similarly in our experiments, Reaction 4 described above is thought to have generated Fe^{2+} , producing H_2O_2 and
385 facilitating the Fenton mechanism Jia et al. (2012); Yap et al. (2011), which would have degraded the adsorbed PAHs,
386 along with direct oxidation by OH radicals and water molecules removed from the clay by UV, and the electron transfer
387 in Reaction 7. Interestingly, only pyrene, fluoranthene, and perylene show degradation in their IR spectra and seem to be
388 significantly affected by this mechanism. Though probably experiencing only weak bonding or long range interactions
389 with the nontronite surface Campisi et al. (2021, 2022), in our experiments pyrene, fluoranthene, and perylene were
390 subject to photodegradation under a dry, hypoxic atmosphere. A summary of the results can be seen in Table 6. The
391 averaged total molecule half-lives and cross sections were compared, and scaled with the average mid-day flux at Gale
392 Crater on Mars of 34.1 Wm^{-2} (in the 200-400 nm range) Vicente-Retortillo et al. (2015); Razzell Hollis et al. (2021),
393 to reflect their significance on the surface of present Mars.

394 Because of their aromaticity, PAHs are inherently stable molecules with large electronic absorption cross-sections,
395 which makes them strong absorbers of UV light. They are also stable as ions, and are thought to be present both
396 positively and negatively charged in the interstellar medium; when PAHs are ionized the strength of modes in their IR
397 spectra involving C-C stretching vibrations can increase manifold, whereas the C-H stretching and, to a lesser extent,
398 the out-of-plane bending vibrations decrease in strength (Tielens, 2008). In our experiments, the spectra of perylene
399 showed evidence of PAH ions, with the formation of new peaks in the C=C range (Figure 4b, c) and a decrease in
400 the C-H band. However, we were not able to determine whether perylene was forming cations or rather undergoing
401 hydrogenation, owing to the difficulty in comparing infrared spectra from our samples with spectra of perylene in the
402 gas phase. The gaps between our understanding of PAH photochemistry in the gas phase, in ice matrices, and in mineral
403 matrices warrant a full-scale analytical campaign.

404 The trends we see in our experiments hold up across the different sample preparation techniques we've used. Our
405 NMR data supports the FTIR data, showing that clay-irradiated pyrene and fluoranthene degraded. The lack of major
406 reaction products in the NMR data could be due to any breakdown products degrading immediately into small volatile
407 hydrocarbons and carbon dioxide (which would not be present in high enough concentrations to cause a change in the
408 spectrum in a DRIFTS type set up). The extraction technique used targeted solid-state products as these are expected to
409 be non-polar given the nature of the parent molecule and the dry, hypoxic experimental conditions. Instead the PAHs
410 may well be degrading directly into CO , CO_2 , C_2H_2 , CH_3OH and other small hydrocarbons, which are volatile and
411 readily escape from the system. This is supported by laboratory results of irradiated PAHs adsorbed to forsterite and
412 anatase, where solid state photodegradation of the PAHs resulted in the production of CO_2 (Potenti et al., 2018).

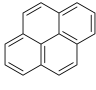
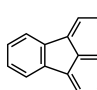
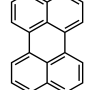


413 Triphenylene and coronene were not degraded by photocatalysis on the surface of nontronite, possibly owing to
414 different binding geometries and adsorption mechanisms between the PAH and the clay surface. If the PAHs are not
415 strongly bound to the surface, they may not be affected by the electron transfer reaction and oxidizing radicals produced
416 by the Fenton mechanism (Reactions 4-7). In general the binding energy increases with the PAH size/surface area, a
417 trend attributed to the increasing number of contact points (though pyrene is an exception to this, having higher binding
418 energies than fluoranthene because of its more compact geometry) (Campisi et al., 2022). Conversely triphenylene in
419 our experiments may have a lower binding energy because of its less compact geometry, facilitating its preservation.
420 Adsorption energies depend also on the specific geometrical interaction of the PAH and the mineral surface, and might
421 not have such a straightforward trend, especially with a complex mineral like nontronite.

422 Triphenylene was shown to degrade when irradiated pure, but was completely preserved when irradiated with
423 nontronite, indicating the clay may be serving in a protective capacity by shielding the PAH from UV radiation.
424 While coronene is stable in pure form, it can be that part of the UV radiation was absorbed by nontronite when they
425 were irradiated together, but its inefficient adsorption to the grains made it immune to the clay's catalytic effects.
426 Alternatively, it is possible a large PAH like coronene with a large electronic absorption cross section absorbed more
427 of the UV radiation, shielding the nontronite and preventing it from forming the required precursors for the Fenton
428 reactions. It is likely the inefficient adsorption of triphenylene and coronene to nontronite grains and/or the large UV
429 absorption capability of coronene are facilitating their deliverance from the photocatalytic effects of nontronite clay.

The photochemical evolution of polycyclic aromatic hydrocarbons and nontronite clay on early Earth and Mars

Table 6

Comparing the effect of nontronite on adsorbed irradiated PAHs. Parameters were calculated with Equations 1-4. The halfives were extrapolated to reflect current surface conditions on Mars, where the average mid-day flux at Gale Crater was calculated using the COMIMART radiative transfer model (Vicente-Retortillo et al., 2015; Razzell Hollis et al., 2021).

PAH	pyrene	fluoranthene	perylene	PAH	triphenylene	coronene
degradation	$C_{16}H_{10}$ 	$C_{16}H_{10}$ 	$C_{20}H_{12}$ 	retention	$C_{18}H_{12}$ 	$C_{24}H_{12}$ 
in the lab where $\Phi = 141 \text{ Wm}^{-2}$ (200-400 nm)						
$t_{d1/2}$ (min)	170±43	72±20	55±17	$t_{f1/2}$ (min)	11±4	4±2
$\sigma_d \times E^{-19}$ (cm ²)	2.0±0.6	6±2	6±2	$\sigma_r \times E^{-19}$ (cm ²)	34±17	79±51
on Mars where $\Phi = 34.1 \text{ Wm}^{-2}$ (200-400 nm)						
$t_{d1/2}$ (sol)	0.5±0.1	0.20±0.06	0.15±0.05	$t_{f1/2}$ (sol)	0.03±0.01	0.012±0.007
effect of nontronite	catalytic	catalytic	catalytic		protective	protective

5. Conclusion

Our UV irradiation experiments of various polycyclic aromatic hydrocarbons (PAHs) adsorbed to nontronite showed both degradation and retention of PAH molecules (Table 6). The degradation of pyrene and fluoranthene was manifested by the decrease of infrared bands and characteristic NMR aromatic peaks. The formation of new peaks in the perylene spectra indicated the formation of perylene cations or hydrogenation of perylene molecules. The triphenylene and coronene IR bands showed no decrease throughout irradiation, indicating the preservation of the molecules. The degradation of PAHs was attributed to the Fenton mechanism resulting from the photocatalytic activity of the irradiated Fe-rich smectite nontronite. Our results indicate the removal of adsorbed and interlayer water from irradiated nontronite, which facilitates the Fenton mechanism and is indicative of processes on Mars, where the observed clays are collapsed, i.e., with no interlayer water. The interlayer water was likely removed from these clays over time, facilitated by the changing environmental conditions, particularly the increasingly harsh radiative environment.

The effect of the Fenton mechanism on PAHs likely depends on their adsorption capacity on nontronite, and their electronic absorption cross section. While nontronite may exhibit both catalytic and protective properties when irradiated with UV, it may also be that PAHs with large electronic cross section can in turn shield nontronite, preventing it from forming the required precursors for the Fenton mechanism. The efficiency of this mechanism thus varies depending on the combination of all these factors, with no straightforward trend. While certain PAHs may have broken down and contributed organic carbon to prebiotic chemistry on clays, others may have remained inert. There exist difficulties in studying PAHs in prebiotic environments, owing to discrepancies in the behavior of infrared spectra between PAHs in experiments like ours and PAHs in the gas phase. The gaps between our understanding of PAH photochemistry in the gas phase, in ice matrices, and in mineral matrices warrant a full-scale analytical campaign.

Assuming the simulated solar spectra used in this study are representative of early Earth, early Mars, and current Mars surface illumination up to 400 nm, the processes occurring in our set up are indicative of the UV-induced photochemistry taking place in Fe-rich clay environments on early Earth and Mars. We have demonstrated that degradation of PAHs on nontronite via the Fenton mechanism is possible, even under a dry, hypoxic atmosphere. Thus certain meteoritic PAHs were likely degraded into smaller organic molecules on the Martian surface, which should be considered when determining the sources of organic molecules detected by Mars rovers. Future organic molecule irradiation experiments in Martian conditions could explore the reactivity of different kinds of smectites, such as Mg-smectites, and sulfates.

Acknowledgements

This work was supported by the Dutch Research Council (NWO) grant ALWOP.274. E.C. is grateful to NWO for an Origins Center Fellowship. The work of M.A.C., G.P., T.F., and J.B. was supported by the Italian Space Agency

The photochemical evolution of polycyclic aromatic hydrocarbons and nontronite clay on early Earth and Mars

461 (ASI) grant agreement ASI/INAF n. 2017-48-H-0. The work of H.v.I. was supported by NWO ENW Roadmap grant
462 00901157 to the uNMRnl consortium. Thanks to two anonymous reviewers for insightful comments and to Andrew
463 Mattioda for fruitful discussions.

464 **Data Availability**

465 The data supplement to this work is freely accessible at <https://public.yoda.uu.nl/geo/UU01/XJOB1.html>,
466 <https://doi.org/10.24416/UU01-XJOB1>.

The photochemical evolution of polycyclic aromatic hydrocarbons and nontronite clay on early Earth and Mars

References

- Adams, J. M., Ballantine, J. A., Graham, S. H., Laub, R. J., Purnell, J. H., Reid, P. I., Shaman, W. Y., and Thomas, J. M. (1979). Selective chemical conversions using sheet silicate intercalates: Low-temperature addition of water to 1-alkenes. *Journal of Catalysis*, 58(2):238–252.
- Basiuk, V., Douda, J., and Navarro-Gonzalez, R. (1999). Transport of extraterrestrial biomolecules to the earth: problem of thermal stability. *Advances in Space Research*, 24(4):505–514.
- Basiuk, V. A. and Navarro-González, R. (1998). Pyrolytic behavior of amino acids and nucleic acid bases: Implications for their survival during extraterrestrial delivery. *Icarus*, 134(2):269–278.
- Bauschlicher, C. W., Ricca, A., Boersma, C., and Allamandola, L. (2018). The nasa ames pah ir spectroscopic database: Computational version 3.00 with updated content and the introduction of multiple scaling factors. *The Astrophysical Journal Supplement Series*, 234(2):32.
- Bernal, J. D. (1949). The physical basis of life. *Proceedings of the Physical Society. Section A*, 62(9):537.
- Bibring, J.-P., Langevin, Y., Gendrin, A., Gondet, B., Poulet, F., Berthé, M., Soufflot, A., Arvidson, R., Mangold, N., Mustard, J., et al. (2005). Mars surface diversity as revealed by the omega/mars express observations. *Science*, 307(5715):1576–1581.
- Boersma, C., Bauschlicher, C., Ricca, A., Mattioda, A., Cami, J., Peeters, E., de Armas, F. S., Saborido, G. P., Hudgins, D., and Allamandola, L. (2014). The nasa ames pah ir spectroscopic database version 2.00: Updated content, web site, and on (off) line tools. *The Astrophysical Journal Supplement Series*, 211(1):8.
- Bristow, T. F., Bish, D. L., Vaniman, D. T., Morris, R. V., Blake, D. F., Grotzinger, J. P., Rampe, E. B., Crisp, J. A., Achilles, C. N., Ming, D. W., et al. (2015). The origin and implications of clay minerals from yellowknife bay, gale crater, mars. *American Mineralogist*, 100(4):824–836.
- Bujdak, J., Slosiarikova, H., Texler, N., Schwendinger, M., and Rode, B. (1994). On the possible role of montmorillonites in prebiotic peptide formation. *Monatshfte für Chemie/Chemical Monthly*, 125(10):1033–1039.
- Cairns-Smith, A. G. (1966). The origin of life and the nature of the primitive gene. *Journal of Theoretical Biology*, 10(1):53–88.
- Campisi, D., Lamberts, T., Dzade, N. Y., Martinazzo, R., Ten Kate, I. L., and Tielens, A. G. (2021). Interaction of aromatic molecules with forsterite: accuracy of the periodic dft-d4 method. *The Journal of Physical Chemistry A*, 125(13):2770–2781.
- Campisi, D., Lamberts, T., Dzade, N. Y., Martinazzo, R., ten Kate, I. L., and Tielens, A. G. (2022). Adsorption of polycyclic aromatic hydrocarbons and c60 onto forsterite: C–h bond activation by the schottky vacancy. *ACS Earth and Space Chemistry*.
- Cannon, K. M., Parman, S. W., and Mustard, J. F. (2017). Primordial clays on mars formed beneath a steam or supercritical atmosphere. *Nature*, 552(7683):88–91.
- Cherchneff, I., Barker, J. R., and Tielens, A. G. (1992). Polycyclic aromatic hydrocarbon formation in carbon-rich stellar envelopes. *The Astrophysical Journal*, 401:269–287.
- Claire, M. W., Sheets, J., Cohen, M., Ribas, I., Meadows, V. S., and Catling, D. C. (2012). The evolution of solar flux from 0.1 nm to 160 μ m: quantitative estimates for planetary studies. *The Astrophysical Journal*, 757(1):95.
- Cnossen, I., Sanz-Forcada, J., Favata, F., Witasse, O., Zegers, T., and Arnold, N. F. (2007). Habitat of early life: Solar x-ray and uv radiation at earth's surface 4–3.5 billion years ago. *Journal of Geophysical Research: Planets*, 112(E2).
- Cockell, C. S. (2000). The ultraviolet history of the terrestrial planets'implications for biological evolution. *Planetary and Space Science*, 48(2-3):203–214.
- Cottin, H., Moore, M. H., and Bénilan, Y. (2003). Photodestruction of relevant interstellar molecules in ice mixtures. *The Astrophysical Journal*, 590(2):874.
- Cruz-Diaz, G. A., Ricca, A., and Mattioda, A. L. (2020). Polycyclic aromatic hydrocarbons and dust particle surface interactions: Catalytic hydrogenation of polycyclic aromatic hydrocarbon molecules under vacuum conditions. *ACS Earth and Space Chemistry*, 4(10):1730–1742.
- Davies, G. F. (1992). On the emergence of plate tectonics. *Geology*, 20(11):963–966.
- Dong, D., Li, P., Li, X., Xu, C., Gong, D., Zhang, Y., Zhao, Q., and Li, P. (2010a). Photocatalytic degradation of phenanthrene and pyrene on soil surfaces in the presence of nanometer rutile tio2 under uv-irradiation. *Chemical Engineering Journal*, 158(3):378–383.
- Dong, D., Li, P., Li, X., Zhao, Q., Zhang, Y., Jia, C., and Li, P. (2010b). Investigation on the photocatalytic degradation of pyrene on soil surfaces using nanometer anatase tio2 under uv irradiation. *Journal of Hazardous Materials*, 174(1-3):859–863.
- dos Santos, R., Patel, M., Cuadros, J., and Martins, Z. (2016). Influence of mineralogy on the preservation of amino acids under simulated mars conditions. *Icarus*, 277:342–353.
- Ehrenfreund, P., Rasmussen, S., Cleaves, J., and Chen, L. (2006). Experimentally tracing the key steps in the origin of life: The aromatic world. *Astrobiology*, 6(3):490–520.
- Eigenbrode, J. L., Summons, R. E., Steele, A., Freissinet, C., Millan, M., Navarro-González, R., Sutter, B., McAdam, A. C., Franz, H. B., Glavin, D. P., et al. (2018). Organic matter preserved in 3-billion-year-old mudstones at gale crater, mars. *Science*, 360(6393):1096–1101.
- Fenton, H. J. H. (1894). Lxxiii.-oxidation of tartaric acid in presence of iron. *J. Chem. Soc., Trans.*, 65:899–910.
- Flynn, G. (1996). Sources of 10 micron interplanetary dust: The contribution from the kuiper belt. In *International Astronomical Union Colloquium*, volume 150, pages 171–175. Cambridge University Press.
- Flynn, G., Keller, L., Jacobsen, C., and Wirick, S. (2004). An assessment of the amount and types of organic matter contributed to the earth by interplanetary dust. *Advances in Space Research*, 33(1):57–66.
- Fornaro, T., Boosman, A., Brucato, J. R., ten Kate, I. L., Siljeström, S., Poggiali, G., Steele, A., and Hazen, R. M. (2018a). Uv irradiation of biomarkers adsorbed on minerals under martian-like conditions: Hints for life detection on mars. *Icarus*, 313:38–60.
- Fornaro, T., Brucato, J. R., Poggiali, G., Corazzi, M. A., Biczysko, M., Jaber, M., Foustoukos, D. I., Hazen, R. M., and Steele, A. (2020). Uv irradiation and near infrared characterization of laboratory mars soil analog samples. *Frontiers in Astronomy and Space Sciences*, 7:539289.
- Fornaro, T., Steele, A., and Brucato, J. R. (2018b). Catalytic/protective properties of martian minerals and implications for possible origin of life on mars. *Life*, 8(4):56.
- Frantseva, K., Mueller, M., ten Kate, I. L., van der Tak, F. F., and Greenstreet, S. (2018). Delivery of organics to mars through asteroid and comet impacts. *Icarus*, 309:125–133.

The photochemical evolution of polycyclic aromatic hydrocarbons and nontronite clay on early Earth and Mars

- 531 Freissinet, C., Glavin, D., Mahaffy, P. R., Miller, K., Eigenbrode, J., Summons, R., Brunner, A., Buch, A., Szopa, C., Archer Jr, P., et al. (2015).
 532 Organic molecules in the sheepbed mudstone, gale crater, mars. *Journal of Geophysical Research: Planets*, 120(3):495–514.
- 533 Frenklach, M. and Feigelson, E. D. (1989). Formation of polycyclic aromatic hydrocarbons in circumstellar envelopes. *The Astrophysical Journal*,
 534 341:372–384.
- 535 Frost, R. L., Klopogge, J. T., and Ding, Z. (2002). The garfield and uley nontronites?an infrared spectroscopic comparison. *Spectrochimica Acta*
 536 *Part A: Molecular and Biomolecular Spectroscopy*, 58(9):1881–1894.
- 537 Fujishima, A., Rao, T. N., and Tryk, D. A. (2000). Titanium dioxide photocatalysis. *Journal of photochemistry and photobiology C: Photochemistry*
 538 *reviews*, 1(1):1–21.
- 539 Gauger, T., Konhauer, K., and Kappler, A. (2015). Protection of phototrophic iron (ii)-oxidizing bacteria from uv irradiation by biogenic iron (iii)
 540 minerals: Implications for early archaean banded iron formation. *Geology*, 43(12):1067–1070.
- 541 Geatches, D., Clark, S., and Greenwell, H. (2012). Iron reduction in nontronite-type clay minerals: Modelling a complex system. *Geochimica et*
 542 *Cosmochimica Acta*, 81:13–27.
- 543 Giese, C.-C., Ten Kate, I. L., Plümper, O., King, H. E., Lenting, C., Liu, Y., and Tielens, A. G. (2019). The evolution of polycyclic aromatic
 544 hydrocarbons under simulated inner asteroid conditions. *Meteoritics & Planetary Science*, 54(9):1930–1950.
- 545 Glavin, D. P., Alexander, C. M., Aponte, J. C., Dworkin, J. P., Elsila, J. E., and Yabuta, H. (2018). The origin and evolution of organic matter in
 546 carbonaceous chondrites and links to their parent bodies. In *Primitive meteorites and asteroids*, pages 205–271. Elsevier.
- 547 Grotzinger, J. P., Sumner, D. Y., Kah, L., Stack, K., Gupta, S., Edgar, L., Rubin, D., Lewis, K., Schieber, J., Mangold, N., et al. (2014). A habitable
 548 fluvio-lacustrine environment at yellowknife bay, gale crater, mars. *Science*, 343(6169).
- 549 Hartman, H. (1975). Speculations on the origin and evolution of metabolism. *Journal of Molecular Evolution*, 4(4):359–370.
- 550 Herzog (2022). Hp-ma: Automatic pulverizing mill. [https://www.herzog-maschinenfabrik.de/en/products/
 551 hp-ma-automatic-pulverizing-mill/](https://www.herzog-maschinenfabrik.de/en/products/hp-ma-automatic-pulverizing-mill/). Accessed: 2019-09-30.
- 552 Huang, W. and Ferris, J. P. (2006). One-step, regioselective synthesis of up to 50-mers of rna oligomers by montmorillonite catalysis. *Journal of*
 553 *the American Chemical Society*, 128(27):8914–8919.
- 554 Hudgins, D. M. and Allamandola, L. (1997). Infrared spectroscopy of matrix-isolated polycyclic aromatic hydrocarbon cations. 4. the tetracyclic
 555 pah isomers chrysenene and 1, 2-benzanthracene. *The Journal of Physical Chemistry A*, 101(19):3472–3477.
- 556 Hudgins, D. M. and Sandford, S. A. (1998). Infrared spectroscopy of matrix isolated polycyclic aromatic hydrocarbons. 1. pahas containing two to
 557 four rings. *The Journal of Physical Chemistry A*, 102(2):329–343.
- 558 Jenniskens, P., Wilson, M. A., Packan, D., Laux, C. O., Krüger, C. H., Boyd, I. D., Popova, O. P., and Fonda, M. (2000). Meteors: A delivery
 559 mechanism of organic matter to the early earth. In *Leonid Storm Research*, pages 57–70. Springer.
- 560 Jia, H., Zhao, J., Fan, X., Dilimulati, K., and Wang, C. (2012). Photodegradation of phenanthrene on cation-modified clays under visible light.
 561 *Applied Catalysis B: Environmental*, 123:43–51.
- 562 Jia, H., Zhao, S., Shi, Y., Zhu, K., Gao, P., and Zhu, L. (2019). Mechanisms for light-driven evolution of environmentally persistent free radicals
 563 and photolytic degradation of pahas on fe (iii)-montmorillonite surface. *Journal of hazardous materials*, 362:92–98.
- 564 Jia, H., Zhao, S., Shi, Y., Zhu, L., Wang, C., and Sharma, V. K. (2018). Transformation of polycyclic aromatic hydrocarbons and formation
 565 of environmentally persistent free radicals on modified montmorillonite: the role of surface metal ions and polycyclic aromatic hydrocarbon
 566 molecular properties. *Environmental science & technology*, 52(10):5725–5733.
- 567 Juntunen, H. L., Leinen, L. J., Pitts, B. K., O'Hanlon, S. M., Theiling, B. P., Barge, L. M., Videau, P., and Gaylor, M. O. (2018). Investigating the
 568 kinetics of montmorillonite clay-catalyzed conversion of anthracene to 9, 10-anthraquinone in the context of prebiotic chemistry. *Origins of Life*
 569 *and Evolution of Biospheres*, 48(3):321–330.
- 570 Keeling, J. L., Raven, M. D., and Gates, W. P. (2000). Geology and characterization of two hydrothermal nontronites from weathered metamorphic
 571 rocks at the uley graphite mine, south australia. *Clays and Clay Minerals*, 48(5):537–548.
- 572 Klopogge, J. T. T. and Hartman, H. (2022). Clays and the origin of life: The experiments. *Life*, 12(2):259.
- 573 Kofman, V., Witlox, M., Bouwman, J., Ten Kate, I., and Linnartz, H. (2018). A multifunctional setup to record ftr and uv-vis spectra of organic
 574 molecules and their photoproducts in astronomical ices. *Review of Scientific Instruments*, 89(5):053111.
- 575 Kumar, B. S., Dhakshinamoorthy, A., and Pitchumani, K. (2014). K10 montmorillonite clays as environmentally benign catalysts for organic
 576 reactions. *Catalysis Science & Technology*, 4(8):2378–2396.
- 577 Laszlo, P. (1987). Chemical reactions on clays. *Science*, 235(4795):1473–1477.
- 578 Lear, P. R. and Stucki, J. W. (1989). Effects of iron oxidation state on the specific surface area of nontronite. *Clays and Clay Minerals*, 37(6):547–552.
- 579 Lecasble, M., Remusat, L., Viennet, J.-C., Laurent, B., and Bernard, S. (2022). Polycyclic aromatic hydrocarbons in carbonaceous chondrites can
 580 be used as tracers of both pre-accretion and secondary processes. *Geochimica et Cosmochimica Acta*, 335:243–255.
- 581 Linsebigler, A. L., Lu, G., and Yates Jr, J. T. (1995). Photocatalysis on tio2 surfaces: principles, mechanisms, and selected results. *Chemical reviews*,
 582 95(3):735–758.
- 583 Liu, R., Xiao, D., Guo, Y., Wang, Z., and Liu, J. (2014). A novel photosensitized fenton reaction catalyzed by sandwiched iron in synthetic nontronite.
 584 *RSC Advances*, 4(25):12958–12963.
- 585 Madejová, J. (2003). Ftr techniques in clay mineral studies. *Vibrational spectroscopy*, 31(1):1–10.
- 586 Marty, B., Alexander, C. M. O., and Raymond, S. N. (2013). Primordial origins of earth's carbon. *Reviews in Mineralogy and Geochemistry*,
 587 75(1):149–181.
- 588 Mattioda, A., Hudgins, D., Boersma, C., Bauschlicher, C., Ricca, A., Cami, J., Peeters, E., de Armas, F. S., Saborido, G. P., and Allamandola, L.
 589 (2020a). The nasa ames pah ir spectroscopic database: the laboratory spectra. *The Astrophysical Journal Supplement Series*, 251(2):22.
- 590 Mattioda, A. L., Cruz-Diaz, G. A., Ging, A., Barnhardt, M., Boersma, C., Allamandola, L. J., Schneider, T., Vaughn, J., Phillips, B., and Ricca,
 591 A. (2020b). Formation of complex organic molecules (coms) from polycyclic aromatic hydrocarbons (pahas): Implications for ism ir emission
 592 plateaus and solar system organics. *ACS Earth and Space Chemistry*, 4(12):2227–2245.
- 593 Moldoveanu, S. C. (2009). *Pyrolysis of organic molecules: applications to health and environmental issues*. Elsevier.

The photochemical evolution of polycyclic aromatic hydrocarbons and nontronite clay on early Earth and Mars

- 594 Murchie, S. L., Seelos, F. P., Hash, C. D., Humm, D. C., Malaret, E., McGovern, J. A., Choo, T. H., Seelos, K. D., Buczkowski, D. L., Morgan,
595 M. F., et al. (2009). Compact reconnaissance imaging spectrometer for mars investigation and data set from the mars reconnaissance orbiter's
596 primary science phase. *Journal of Geophysical Research: Planets*, 114(E2).
- 597 Nagendrappa, G. et al. (2002). Organic synthesis using clay catalysts: clays for ?green chemistry? *Resonance-journal of science education*, 7(1).
- 598 Ohno, T., Tokieda, K., Higashida, S., and Matsumura, M. (2003). Synergism between rutile and anatase tio₂ particles in photocatalytic oxidation
599 of naphthalene. *Applied Catalysis A: General*, 244(2):383–391.
- 600 Okumura, F. and Mimura, K. (2011). Gradual and stepwise pyrolyses of insoluble organic matter from the murchison meteorite revealing chemical
601 structure and isotopic distribution. *Geochimica et Cosmochimica Acta*, 75(22):7063–7080.
- 602 O'Neil, J., Carlson, R. W., Francis, D., and Stevenson, R. K. (2008). Neodymium-142 evidence for hadean mafic crust. *Science*, 321(5897):1828–
603 1831.
- 604 Pearson, V. K., Sephton, M. A., Kearsley, A. T., Bland, P. A., Franchi, I. A., and Gilmour, I. (2002). Clay mineral-organic matter relationships in
605 the early solar system. *Meteoritics & Planetary Science*, 37(12):1829–1833.
- 606 Pendleton, Y. J. and Allamandola, L. J. (2002). The organic refractory material in the diffuse interstellar medium: Mid-infrared spectroscopic
607 constraints. *The Astrophysical Journal Supplement Series*, 138(1):75.
- 608 Pierson, B. K., Mitchell, H. K., and Ruff-Roberts, A. L. (1993). Chloroflexus aurantiacus and ultraviolet radiation: implications for archean shallow-
609 water stromatolites. *Origins of Life and Evolution of the Biosphere*, 23(4):243–260.
- 610 Poch, O., Jaber, M., Stalport, F., Nowak, S., Georgelin, T., Lambert, J.-F., Szopa, C., and Coll, P. (2015). Effect of nontronite smectite clay on the
611 chemical evolution of several organic molecules under simulated martian surface ultraviolet radiation conditions. *Astrobiology*, 15(3):221–237.
- 612 Poggiali, G., Fornaro, T., Potenti, S., Corazzi, M. A., and Brucato, J. R. (2020). Ultraviolet photoprocessing of glycine adsorbed on various space-
613 relevant minerals. *Frontiers in Astronomy and Space Sciences*, 7:18.
- 614 Potenti, S., Manini, P., Fornaro, T., Poggiali, G., Crescenzi, O., Napolitano, A., Brucato, J. R., Barone, V., and d'Ischia, M. (2018). Solid
615 state photochemistry of hydroxylated naphthalenes on minerals: probing polycyclic aromatic hydrocarbon transformation pathways under
616 astrochemically-relevant conditions. *ACS Earth and Space Chemistry*, 2(10):977–1000.
- 617 Poulet, F., Carter, J., Bishop, J., Loizeau, D., and Murchie, S. (2014). Mineral abundances at the final four curiosity study sites and implications for
618 their formation. *Icarus*, 231:65–76.
- 619 Razzell Hollis, J., Fornaro, T., Rapin, W., Wade, J., Vicente-Retortillo, Á., Steele, A., Bhartiya, R., and Beegle, L. W. (2021). Detection and
620 degradation of adenosine monophosphate in perchlorate-spiked martian regolith analog, by deep-ultraviolet spectroscopy. *Astrobiology*,
621 21(5):511–525.
- 622 Remusat, L., Derenne, S., Robert, F., and Knicker, H. (2005). New pyrolytic and spectroscopic data on orgueil and murchison insoluble organic
623 matter: A different origin than soluble? *Geochimica et Cosmochimica Acta*, 69(15):3919–3932.
- 624 Ruppert, G., Bauer, R., and Heisler, G. (1993). The photo-fenton reaction as an effective photochemical wastewater treatment process. *Journal*
625 *of Photochemistry and Photobiology A: Chemistry*, 73(1):75 – 78.
- 626 Scappini, F., Casadei, F., Zamboni, R., Franchi, M., Gallori, E., and Monti, S. (2004). Protective effect of clay minerals on adsorbed nucleic acid
627 against uv radiation: possible role in the origin of life. *International Journal of Astrobiology*, 3(1):17–19.
- 628 SDBS (2022). SDBSWeb. <https://sdbws.db.aist.go.jp>. Accessed: 2020-09-30.
- 629 Sephton, M. A. (2002). Organic compounds in carbonaceous meteorites. *Natural product reports*, 19(3):292–311.
- 630 Shkrob, I. A. and Chemerisov, S. D. (2009). Light induced fragmentation of polyfunctional carboxylated compounds on hydrated metal oxide
631 particles: from simple organic acids to peptides. *The Journal of Physical Chemistry C*, 113(39):17138–17150.
- 632 Shkrob, I. A., Marin, T. M., Adhikary, A., and Sevilla, M. D. (2011a). Photooxidation of nucleic acids on metal oxides: Physicochemical and
633 astrobiological perspectives. *The Journal of Physical Chemistry C*, 115(8):3393–3403.
- 634 Shkrob, I. A., Marin, T. W., Chemerisov, S. D., and Sevilla, M. D. (2011b). Mechanistic aspects of photooxidation of polyhydroxylated molecules
635 on metal oxides. *The Journal of Physical Chemistry C*, 115(11):4642–4648.
- 636 Sýkora, J. (1997). Photochemistry of copper complexes and their environmental aspects. *Coordination Chemistry Reviews*, 159:95–108.
- 637 Szczepanski, J., Chapo, C., and Vala, M. (1993). Visible and infrared spectra of matrix-isolated perylene cations. *Chemical physics letters*, 205(4-
638 5):434–439.
- 639 ten Kate, I. L., Garry, J. R., Peeters, Z., Quinn, R., Foing, B., and Ehrenfreund, P. (2005). Amino acid photostability on the martian surface.
640 *Meteoritics & Planetary Science*, 40(8):1185–1193.
- 641 Theng, B. K. (2018). *Clay mineral catalysis of organic reactions*. CRC press.
- 642 Thomson, B., Bridges, N., Milliken, R., Baldrige, A., Hook, S., Crowley, J., Marion, G., de Souza Filho, C., Brown, A., and Weitz, C. (2011).
643 Constraints on the origin and evolution of the layered mound in gale crater, mars using mars reconnaissance orbiter data. *Icarus*, 214(2):413–432.
- 644 Tielens, A. (2013). The molecular universe. *Reviews of Modern Physics*, 85(3):1021.
- 645 Tielens, A. G. (2008). Interstellar polycyclic aromatic hydrocarbon molecules. *Annu. Rev. Astron. Astrophys.*, 46:289–337.
- 646 Tu, V. M., Rampe, E. B., Bristow, T. F., Thorpe, M. T., Clark, J. V., Castle, N., Fraeman, A. A., Edgar, L. A., McAdam, A., Bedford, C., et al. (2021).
647 A review of the phyllosilicates in gale crater as detected by the chemin instrument on the mars science laboratory, curiosity rover. *Minerals*,
648 11(8):847.
- 649 Vicente-Retortillo, A., Martínez, G., Rennó, N. O., Lemmon, M., de la Torre-Juárez, M., and Gómez-Elvira, J. (2020). In situ uv measurements by
650 msl/rem:s dust deposition and angular response corrections. *Space Science Reviews*, 216(5):1–19.
- 651 Vicente-Retortillo, Á., Valero, F., Vázquez, L., and Martínez, G. M. (2015). A model to calculate solar radiation fluxes on the martian surface.
652 *Journal of Space Weather and Space Climate*, 5:A33.
- 653 Wang, Y., Liu, C., Li, F., Liu, C., and Liang, J. (2009). Photodegradation of polycyclic aromatic hydrocarbon pyrene by iron oxide in solid phase.
654 *Journal of Hazardous Materials*, 162(2-3):716–723.
- 655 Wen, S., Zhao, J., Sheng, G., Fu, J., et al. (2002). Photocatalytic reactions of phenanthrene at tio₂/water interfaces. *Chemosphere*, 46(6):871–877.

The photochemical evolution of polycyclic aromatic hydrocarbons and nontronite clay on early Earth and Mars

- 656 Whittet, D. (1997). Is extraterrestrial organic matter relevant to the origin of life on earth? In *Planetary and Interstellar Processes Relevant to the*
657 *Origins of Life*, pages 249–262. Springer.
- 658 Yap, C. L., Gan, S., and Ng, H. K. (2011). Fenton based remediation of polycyclic aromatic hydrocarbons-contaminated soils. *Chemosphere*,
659 83(11):1414–1430.
- 660 Zhang, L., Li, P., Gong, Z., and Li, X. (2008). Photocatalytic degradation of polycyclic aromatic hydrocarbons on soil surfaces using tio₂ under uv
661 light. *Journal of Hazardous Materials*, 158(2-3):478–484.
- 662 Zhang, L., Xu, C., Chen, Z., Li, X., and Li, P. (2010). Photodegradation of pyrene on soil surfaces under uv light irradiation. *Journal of Hazardous*
663 *Materials*, 173(1-3):168–172.